Journal of Physics:
Conference Series

PAPER • OPEN ACCESS

Digitalization of the urban communities: energy harvesting from water pipeline to enhance leakage monitoring and detection

To cite this article: Ravi Nath Tiwari *et al* 2024 *J. Phys.: Conf. Ser.* **2893** 012122

Digitalization of the urban communities: energy harvesting from water pipeline to enhance leakage monitoring and detection

Ravi Nath Tiwari[1], Tatiana Pais[2*], Federico Reggio[1], Matteo Pascenti[3], Alberto Traverso[1], Paolo Silvestri[1]

[1] University of Genoa, Department of Mechanical Engineering, Thermochemical Power Group, via Opera Pia 15, 16145 Genoa, Italy
[2] University of Genoa, Department of Naval Architecture and Marine Engineering, via Opera Pia 11A, 16145 Genoa, Italy
[3] SIT Technologies Srl, Genova, Italy

*E-mail: tatiana.pais@unige.it

Abstract. The SMART PIPING project aims to design, create and test innovative solutions for resilience of water and energy networks, aiming to develop technologies for the energy autonomy of stations monitoring of infrastructures suitable for the transport of fluids (natural gas and biogas, hydrocarbons, water). In this paper, an innovative bladeless turbine is designed and manufactured in relevant environment to demonstrate the feasibility of harvesting significant amount of energy in the urban pipeline distribution network to power local devices to monitor the piping health and enable leakage early-warning. Results show that bladeless turbine can constitute a cost-effective and highly reliable device to enable the digital and energy-efficient transition of urban communities.

KEYWORDS: Bladeless turbine, Tesla expander, computational fluid dynamics, Energy harvesting, Small turbomachinery

1. Introduction

Water pipeline networks are crucial components of urban infrastructure. However, they face several challenges that affect their efficiency, reliability, and sustainability. The most prominent problems include leakage (causing water loss), corrosion (material degradation), pressure management, aging infrastructure, environmental impact, etc. To meet these challenges, it is necessary to combine technological innovations, such as the integration of smart sensors and energy-harvesting systems, with investments in infrastructure upgrades and proactive maintenance techniques. It is essential to adopt advanced technologies to optimize infrastructure and improve quality of life for urban communities as part of the digitalization process. Energy harvesting from smart water pipelines is one of the most significant innovations in this field. This pipeline is equipped with water turbines in order to reduce maintenance costs and provide power for the operation of sensors and monitoring devices. It should be noted, however, that the main characteristics of conventional turbine performance decreased with regard to scaling size, while bladeless or Tesla turbine performance remains almost constant [1]. Furthermore, Tesla technologies have several attractive characteristics, including ease of construction, low maintenance, low noise, affordability, and reversibility[1][2].

Tesla patented bladeless pumps and turbines in 1909 and 1911, utilizing the boundary layer principle, with both patents granted in 1913[3][4]. Due to this innovation, the technology is referred to as Tesla-type turbomachinery. Currently, there is significant demand for devices that are affordable, efficient, compact, reversible, and low noise, particularly on a small scale. Tesla or bladeless technologies meet these requirements [5][6]. This turbomachinery offers several advantages, including reversible operation, low cost, suitability for dirty fluids, and lower noise levels compared to conventional devices [5][8][9][9][10][11].

A Tesla machine consists of thin disks mounted on a shaft with spacers, collectively known as the Tesla rotor. As illustrated in Figure 1, the rotor assembly is housed in a cylindrical volute casing with a locking plate and bearing to secure the shaft. In turbine compressor mode (indirect mode), fluid enters axially, flows spirally through the disk gaps, and exits radially through the volute, absorbing mechanical energy from the shaft. When operating in mode (direct mode), the flow and angular speed reverse, converting pressure head into mechanical energy extractable from the shaft. Rice, a leading researcher in Tesla technologies, noted that while conventional devices' performance degrades when scaled down, Tesla machines maintain consistent performance[7]. Rice's bladeless rotor for the Tesla compressor featured 77 disks with an outer radius of 75 mm, each disk being 0.5 mm thick with a 0.5 mm gap. Experimental results showed 23% efficiency at 20,000 rpm and a mass flow rate of 101 g/s.

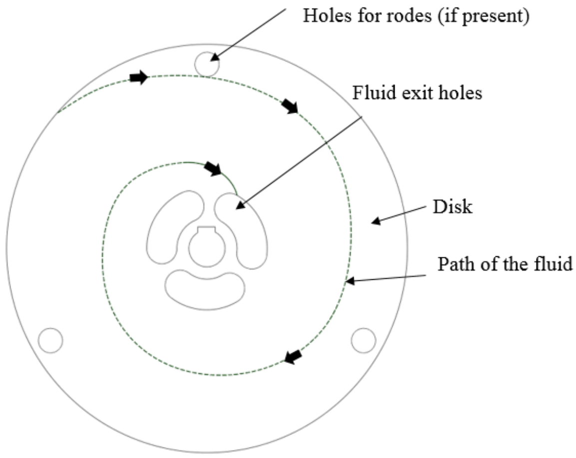

Figure 1: A Tesla turbine rotor and fluid path inside disk gap and principle of operation

The turn of the 20th century saw exponential growth in research on compact, lightweight, and efficient bladeless technologies [8][9]. Tesla technologies present a viable alternative to micro-conventional turbomachinery, with opportunities in niche markets such as Tesla pumps, blood pumps, and expanders. Tesla-type pumps are available globally for micro applications, although further research is needed to enhance system reversibility and efficiency. The University of Genova spinoff company SIT Technologies Srl has developed several prototype models [12]. A 3-kW air expander with an outer diameter of 120 mm and 0.1 mm disk thickness achieved 36.5% isentropic efficiency—the highest experimental efficiency recorded with air as the working fluid—while numerical analysis indicated 58% efficiency without assembly losses [8]. Loss characterization demonstrated significant impacts from end-wall leakage and ventilation losses [13]. Tesla technologies can function as both an expander and a compressor without major modifications. Tiwari [8] numerically simulated a 3-kW expander in compressor mode and validated the results experimentally at various rotational speeds, measuring a pressure ratio of 1.15-1.25 at 20,000 and 30,000 rpm, indicating the prototype's potential as a blower [8]. Additionally, vibro-acoustic analysis showed that bladeless devices have significantly lower noise emissions than bladed devices [5].

For optimal performance, the disk gap should be three times the boundary layer thickness, with Ekman numbers around 1.5-1.6 and Reynolds numbers between 9-11 [14]. According to Tiwari's numerical results, the disk diameter ratio should be between 2.5 and 4.5 for maximum efficiency in compressor mode. Larger diameters increase efficiency at low mass flow rates but decrease sharply at higher mass flow rates [15].

This paper presents the design and manufacture of an innovative bladeless, or Tesla, turbine in a relevant environment for energy harvesting. The harvester has been developed for SMART PIPING project, which aims to design, develop, and test innovative solutions to enhance the resilience of water and energy networks. It focuses on creating technologies for the energy autonomy of monitoring stations for infrastructures transporting fluids such as natural gas, biogas, hydrocarbons, and water.

The goal is to demonstrate the feasibility of harvesting significant energy from urban pipeline distribution networks to power local devices for monitoring pipeline health and enabling early leakage warnings. The results indicate that the bladeless turbine is a cost-effective, robust and highly reliable device, supporting the digital and energy-efficient transition of urban communities. In the following is a description of the reversible Tesla machine for this application.

2. Requirements for water pipeline monitoring stations

Usually, pipelines need monitoring stations to verify their health: these are transducers that monitors pressures, mass-flows, temperatures to ensure that all the parameters are inside the normal intervals; when variations arise, there is a problem on the pipelines (leakage, occlusion…). These transducers need some electrical power to work, it's not too much, but it's required locally for every section of some length of the pipeline, and sometimes monitoring stations are very far from power lines, so the idea is to use the pressure of the medium to extract the needed power.

In the SMART PIPING project, the water turbine generators will be applied to water pipeline networks, which are usually constituted by a pump that moves water to a main reservoir located at the maximum height of the pipeline and a series of other secondary reservoirs located along the path. This configuration breaks the total water head to a value compatible with the components and users located into the single pipeline segment.

The required power for each monitoring station it's less than 1 kW, so the generator machine will be not too big; in terms of rotational speed, because the low maximum velocity achievable with water, this will be low, so the generator needs a high voltage/rpm factor and a high number of poles.

The voltage generated will be variable for the whole span from zero to maximum, so it's required a converter (AC or DC) to obtain a constant voltage; usually for industrial transducers the required voltage is around 24V (AC or DC), so it's possible to use a low voltage-high current generator.

These generators feature a low number of coils and large section of winding, so the ohmic losses will be low and with good efficiencies. With water as medium, it is possible to cool the generator easily through a water jacket.

3. Design of turbine – rotor and volute

3.1. Design of rotor

Nikola Tesla invented the bladeless turbine for which he claimed 97% efficiency, although it has not been tested and proven. Tiwari[15] asserts that such efficiencies are only possible under optimal design conditions for independent rotors at very low mass flow rates. Tiwari indicated in his numerical studies that the optimal disk gap should be three times the thickness of the boundary layer, and the disk diameter ratio should range between 2.5 and 4.5 [14]. Because of frictional losses associated with larger stator or volute areas, efficiency has been reduced in both stator and volute configurations. However, as much as possible minimum area of stator or statorless configuration should be beneficial to obtain better performance.
Based on the urban pipeline network pressure, Telsa turbine speed has been finalized, and disk diameter and disk gap have been adjusted accordingly. Because the Tesla rotor is at the heart of Tesla technologies, it has been considered how to determine the optimal disk gap parameter; however, Rice [9], who is a very prominent figure in Tesla history, suggested that the disk gap should be twice the boundary layer thickness and that the Reynolds number should be between 5 and 6, as indicated in Eq.1. According to Tiwari et al., the optimal gap between disks can be determined using the Ekman number, where the optimal Reynolds number should be 9-11 and the optimal Ekman number should be 1.5-1.6. For this case, the disk gap should be three times the thickness of the boundary layer, which is determined by equations 1 and 2.

$$Re = \frac{\omega(2h)^2}{\upsilon} \qquad 1$$

$$E_k = \frac{h}{\delta} = h * (\sqrt{\omega/\upsilon}) \qquad 2$$

The disk gap has been examined at different speeds based on Tiwari and Rice's studies, which are shown in dark bold and normal text respectively in Table 1. The disk gap varies with speed, and it is higher at lower speed and increasing the speeds it's decrease. Considering the turbine design speed of 1800 rpm, the disk gap should be 0.22mm, however the best practicable disk gap of 0.2mm has been considered, which falls within the optimal range. The rotor pack can be seen in Figure 2 (left)

Table 1: Disk gap estimation at different rotational speed based on Tiwari (bold) and Rice (without bold) estimations

Speed (rpm)	**Ekman Number**	**Disk gap (2h_mm)**	**Re Number (ω*2h*2h/υ)**
1500	**1.60**	**0.242**	**10.24**
1500	1.20	0.181	5.76
1800	**1.60**	**0.221**	**10.24**
1800	1.20	0.166	5.76
2000	**1.60**	**0.210**	**10.24**
2000	1.20	0.157	5.76
2500	**1.60**	**0.187**	**10.24**

2500	1.20	0.141	5.76

3.2 Design of Volute

Past studies by the author indicate that the performance of the system is better with a statorless configuration (volute) when air is considered as the fluid [15]. The losses are primarily due to frictional losses on the skin, which adversely affect the turbine overall performance. To minimize skin effect losses, the shape of a bladeless compressor's volute is examined to gain a better understanding of its performance. As the author reviewed past studies of the relevant information, it became evident that frictional losses are higher immediately following the stator or volute throat; therefore, it is essential to maintain the optimal volute area. While SIT technologies demonstrated better performance with incompressible fluids (water) both numerically and experimentally through the use of a volute configuration. As a way to design the most optimal and efficient Tesla turbine, statorless configuration has been considered for the water turbine for the pipeline network, which has been evaluated using simple calculations based on conservation of mass and momentum. The volute shape can be seen in Figure 2 (right).

4. Numerical analysis

To perform the CFD analysis of the Tesla or bladeless turbine, Ansys fluent commercial software has been used. The performance has evaluated based on the CFD results which has post processing using the mass weighted average method.

4.1 Geometrical data and CFD boundary conditions

An innovative bladeless or Tesla turbine has been designed in accordance with optimal design parameters which allows it to demonstrate the feasibility of harvesting significant amounts of energy in the urban pipeline distribution network for powering local devices. The geometrical parameters of the Tesla turbine (M-3) are shown in Table 2.

Table 2: Geometrical parameter of Tesla water turbine (M-3)

Parameters	M-3
Disk outer diameter (2*r_o), mm	120
Disk inner diameter (2*r_i), mm	40
Disk diameter, ratio	3
Disk thickness, mm	0.1
Disks gap (2h), mm	0.2
Reynolds number (Ek)	9 (1.5)
Number of disk gap	55
Volute outer diameter, mm	132
Volute inlet duct, mm	8.4
Throat, mm	5.7
Rotational speed (krpm)	1.8

For this model, the name "M-3" is used, which refers to the diameter ratio of 3. The outer diameter of the disk is 120 mm, while the inner diameter is 40 mm. The gap between disks of model "M-3" is 0.2 mm, and the disk thickness is 0.1 mm. It consists of a combination of disks and disk gaps attached to drive rods to form a rotor. Two thicker disks provide the mechanical integrity to this thin disk rotor pack, which is packaged in sandwich form can be seen Figure 2 (left). Based on the power requirement, a disk gap number of 55 is considered considering losses (end wall frictional losses, leakage) as well which will be present in the actual prototype. A lower speed has been considered in order to minimize the frictional losses at the end wall, which indicated that the frictional losses would be lower at a lower speed. In accordance with literature surveys, Tesla machines generally operate at a high speed, however, end wall frictional losses are higher that influence the overall performance of the machine. The statorless configuration with an outer diameter of 132 mm and a throat diameter of 5.7 mm was chosen in order to obtain the best performance. The Tesla turbine M-3 rotor (left) and volute (right) are shown in Figure 2.

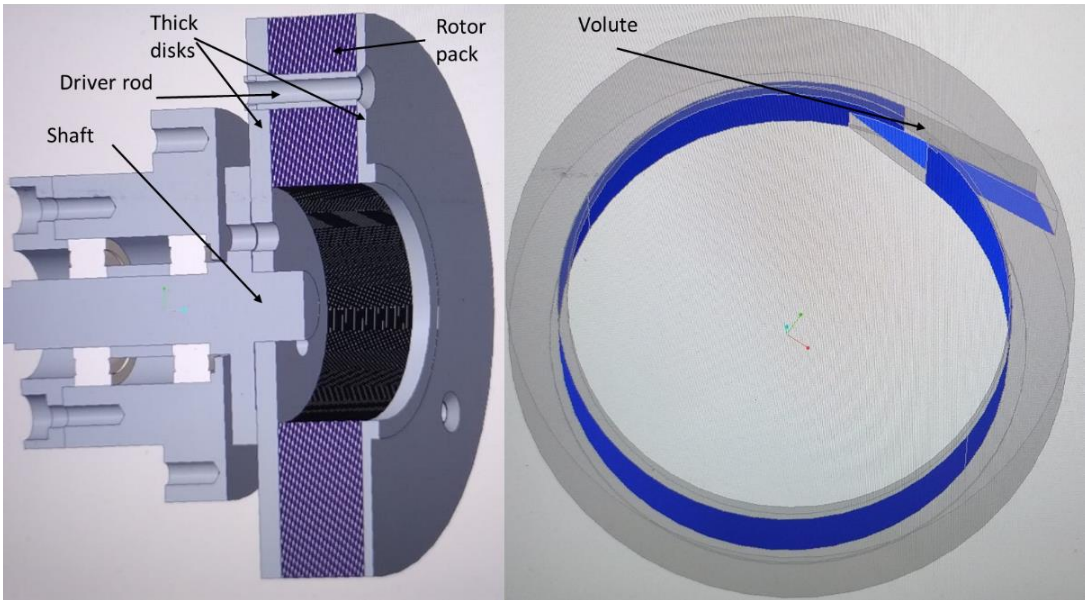

Figure 2: Tesla water turbine: rotor model (left) and volute mode (right)

There has been a consideration of the boundary conditions for the mass flow inlet and static pressure outlet during the CFD analysis. As can be seen in Figure 3, a CFD boundary condition is applied to the geometry. In the CFD analysis, a single fluid domain of a coupled rotor-volute configuration has been considered.

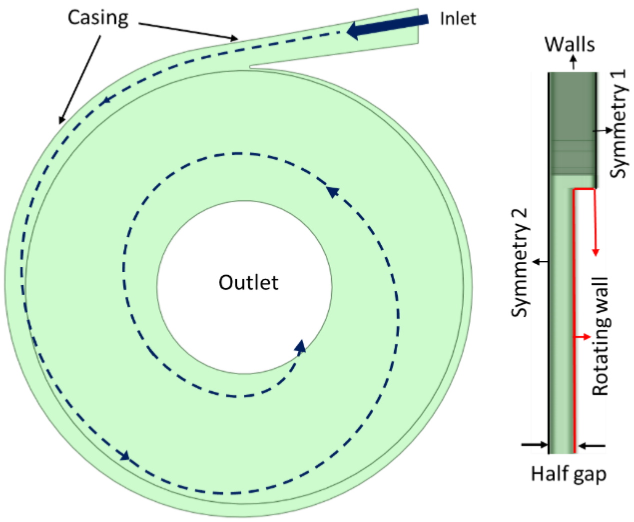

Figure 3: Tesla water turbine: CFD boundary condition for coupled rotor-volute singe fluid domain

As can be seen in Figure 3, a CFD boundary condition has been set for half of the disk thickness and half of the disk gap between rotating disks. Symmetry 1 is applied to the volute side and symmetry 2 is applied to the centre of the disk gap and volute. A rotating wall is applied to a rotating surface indicated by a red line, whereas a stationary wall corresponds to a stationary surface. As a moving wall, the rotating wall is considered to be no-slip. Both stationary and moving walls are considered using the standard roughness model (sand-grain roughness constant equal to 0.5). A total of five layers of inflation are applied to both stationary and mobile walls.

4.2 Numerical Set-up

The numerical analysis is performed using the commercial software Ansys Fluent. Two types of solvers are offered by Ansys: pressure-based solvers and density-based solvers. Pressure-based solvers have been developed for incompressible fluids, whereas density-based methods have been developed for highly compressible fluids [16]. It has been demonstrated, however, that pressure-based solvers are more stable than density-based solvers when dealing with highly compressible flows in turbomachinery [17]. This paper uses a pressure-based steady solver to solve steady and incompressible flows using water as the working fluid. RANS models defined by a pair of equations are the most used. Compared to other turbulence models, SST (shear stress transport) turbulence models offer an excellent trade-off between computation cost and accuracy, as demonstrated by Menter's [18] model. Using the SST model, it is possible to combine the robust and accurate formulation of the k-w model [17][18] in the near-wall region with the free-stream independence of the k-ω model in the far field (Menter, 1992) [18]. The k-ω SST viscous model is selected in this numerical study. The governing equations are solved using a coupled scheme for fluid coupling of pressure and velocity. Coupled schemes have some advantages over non-coupled schemes. For steady-state flows, this scheme offers a robust and efficient single-phase implementation, which performs better than segregated schemes. A second-order linear interpolation upwind approach is used in this scheme. As recommended by the k-w SST model, the facet average wall function y+ values are maintained. It is recommended to use a y+ value of less than 1 for this k-w SST model, but this value may be less than 5 depending on the complexity of the model. It is noteworthy, however, that in this analysis, the y+ value is less than 1 at moving walls, while it is less than 3 at stationary walls. The y+ parameter is maintained in accordance with the k-ω SST model. A mass flow rate inlet is set at the volute inlet boundary, whereas a static pressure outlet boundary is applied at the rotor exit for this CFD analysis.

For the mesh analysis, the grid is generated in tetrahedral mesh using Ansys software and it is converted in polyhedral mesh using Ansys fluent software can be seen in Figure *4*. It has become increasingly popular to use polyhedral meshes in computational geometry, and numerical simulations due to their numerous advantages over traditional tetrahedral and hexahedral meshes. Here are some of the key benefits: Flexibility in mesh generation, Improved computational efficiency, Enhanced simulation accuracy and fast convergence. The grid sensitivity has been analysed using four mesh models, best possible lowest error mesh model has been considered that have error less than 1% in torque and pressure. This mesh model consists of approximately 640,719 cells.

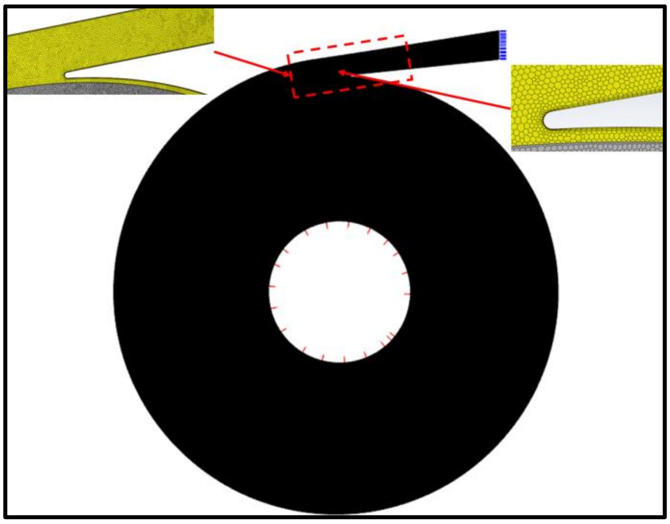

Figure 4: Tesla water turbine: Mesh distribution for coupled rotor-volute singe fluid domain

4.3 Numerical Results

The numerical analysis is conducted for the Tesla turbine with incompressible fluid water. This section discusses the performance analysis of the Tesla turbine at various inlet pressure. Figure 5 illustrates the Tesla turbine pressure verses mass flow rate at design speed 1800 rpm. This machine has been designed to operate at 1.5 l/s mass flow rate where pressure drop should be 2 bar. However, CFD analysis has been conducted at different mass flow rate, which is shown increasing mass flow rate, pressure difference is increases. At 1.5 l/s the pressure difference is around 2.2 bar. This CFD results showing performance without losses consideration i.e., leakage and end wall frictional losses which will be present in real prototype.

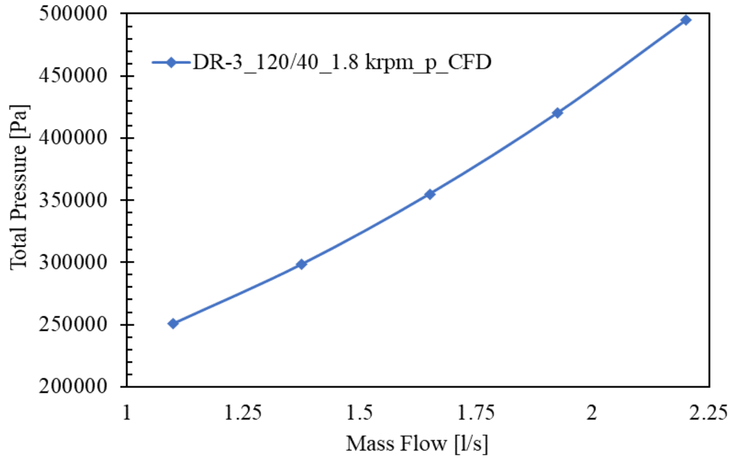

Figure 5: Total pressure and mass flow rate of the Tesla turbine, CFD results (exit pressure set at 105 Pa)

As illustrated in Figure 6, power and total to total efficiency are plotted in relation to mass flow rate. On the y-axis, power is plotted at the primary axis, while efficiency is plotted at the secondary axis. Power is a function of mass flow rate, which increases as the mass flow rate increases. The relationship between power and mass flow rate is directly proportional. This means that as the mass flow rate increases, the power output also increases. This is because a higher mass flow rate allows for more energy to be transferred and converted into power. There is a power of approximately 200 W at a design mass flow rate of 1.5 l/s, where the pressure drop is approximately 2.2 bar. Power is calculated using Eq. 3, which is the multiplication of torque and omega. Compared to conventional turbines, Tesla turbines performed better at low mass flow rates, which was expected, however, increasing the mass flow rate was abandoned due to inefficiency. The total-to-total efficiency has been determined by Eq 4 and 5, which illustrates it is the ratio between the output and the input power. An efficiency of 75.5% was achieved at a mass flow rate of 1.10 l/s with turbines predicted to produce 115 watts. As the mass flow rate increases from 1.1 to 2.2 l/s, efficiency drops by around 17% from 75.5% to 58.5%, mainly due to frictional and pressure losses. The frictional losses in the turbine have a significant impact on its overall efficiency. As the mass flow rate increases, these losses become more pronounced, leading to turbine efficiency decrease. This is because frictional forces between the moving parts of the turbine, as well as with the surrounding surfaces, result in energy being converted into heat and lost from the system. Therefore, reducing frictional losses through improved design and materials is crucial for maximizing turbine efficiency. It has been predicted that the CFD results would predict very high efficiency without accounting for losses, however, the actual prototypes are likely to have lower efficiency due to frictional losses at the end walls and leakage during operation.

$$P_{bh-cfd} = \tau * \omega \qquad 3$$

$$\eta_{t-t} = \frac{P_{bh}}{P_{wh}} = \frac{\tau * \omega}{W * Q * H_{net}} \qquad 4$$

$$W = \rho * g \qquad 5$$

Where P_{bh-cfd} represent the brekadown horsepower, P_{wh} is the water horsepower, Q is the volume flow rate, and H_{net} is the net head.

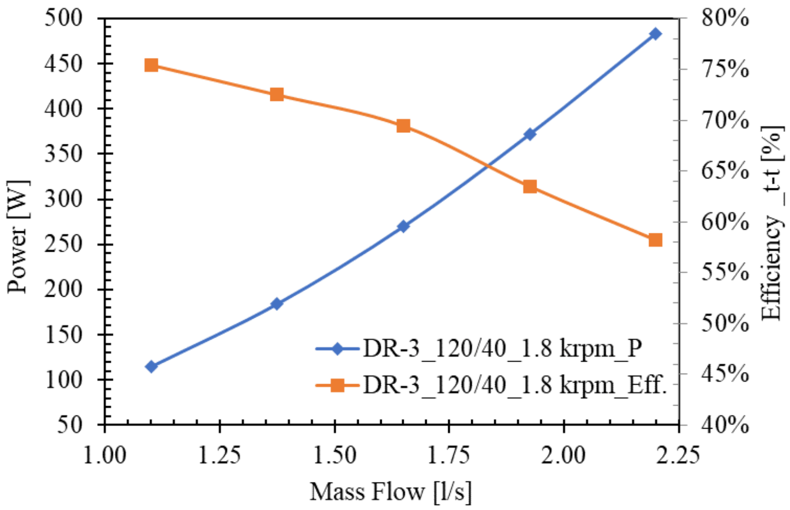

Figure 6: Tesla turbine performance: Power (primary y axis), efficiency (secondary y axis) vs mass flow rate

In 2003, Gulich elucidated end wall frictional losses by utilizing equations 6, 7 and 8. The same theoretical model has been used to evaluate the frictional losses on the end walls of this water turbine M3. It has been assumed that the gap between the end walls (S_{ax}) is 1mm. In this equation, P_{RR} represents frictional power loss, k_{RR} represents frictional factor, and Re represents Reynolds number.

$$P_{RR} = \frac{k_{RR}}{Cos\delta}\rho\omega^3 r_o^5 \left\{1 - \left(\frac{r_i}{r_o}\right)^5\right\} \qquad 6$$

$$k_{RR} = \frac{0.0255}{Re^{0.2}}(S_{ax}^*)^{0.1}\ ; \qquad Re > 2 * 10^5 \qquad 7$$

$$Re = \frac{\omega r_o^2}{\upsilon}\ ; \qquad S_{ax}^* = S_{ax}/r_o \qquad 8$$

In this case, the end wall frictional losses are estimated to be around 8 W per side with zero leakage; however, when both sides have net zero leakage, the frictional power is estimated to be around 16 Watts. As a result of considering this frictional loss of both end wall sides, the total-to-total efficiency will be 65.5% which is approximately 10 percentage points lower than the overall efficiency (without considering losses due to rotor leakage, bearings, electrical efficiency).

5. Turbine mechanical components

This section presents a summary description of mechanical components of the designed bladeless tesla expander. The main structural parts of the water turbine are visualize in Figure 2. The Tesla turbine is designed to operate at speeds up to 1.8 krpm. Given the need to seal the turbine casing, the rotor has a cantilevered (as shown in Figure 2left and Figure 7) and a magnetic joint has been enployed to trasmit the torque to the electric generator keeping the shaft inside the casing and avoiding the water exit. The rotor is supported by two spindle bearings: the bearings are supported and kept aligned in a single aluminium cartridge that can be removed for maintenance from the casing flanges. On the opposite side, the cantilever disc pack is bolted to a small flange welded to the shaft that has been turned and ground together with it.

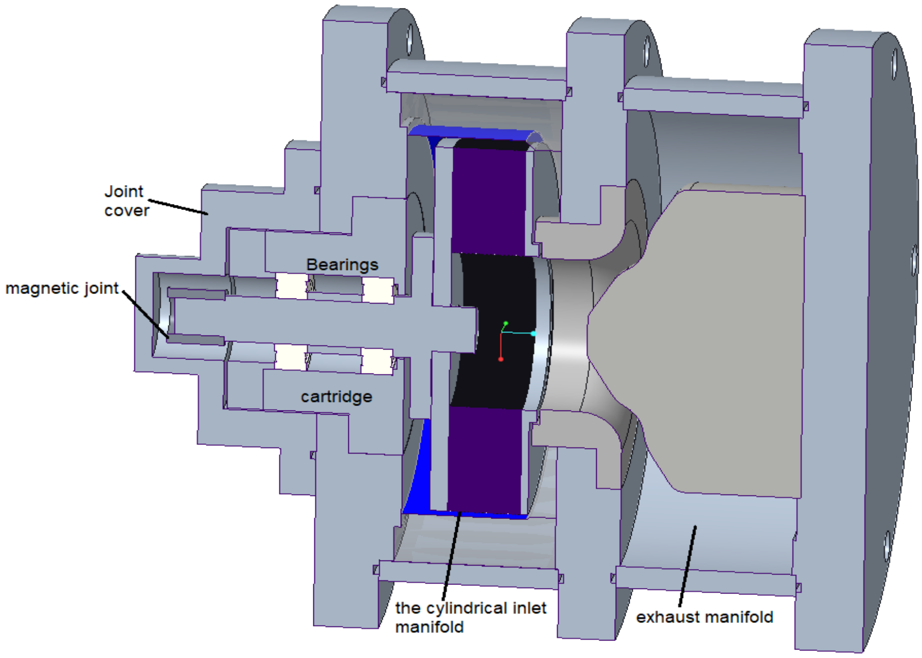

Figure 7: Whole turbine section

The turbine has two chambers: the cylindrical inlet manifold, which is connected externally to the two inlet pipes, and the chamber containing the rotating disks. The liquid that comes out of the turbine is collected in an exhaust manifold and exits from the pipe drain. All the machine components are held together by flanges and six threaded rods with a 8 mm diameter. Figure 2 (left and right) shows the Tesla rotor and volute type casing assembly. The volute type statorless casing is made from both plastic and metal using 3D printing technology. The figure also shows the complete CAD model of the expander with inlet and exhaust piping arrangements.

Conclusions

This work presents a numerical design study of a Tesla turbine prototype under construction. To achieve this, a bladeless rotor has been paired with a bladeless stator within a volute-type casing. Evaluating the overall efficiency of this Tesla device, excluding overall assembly losses (such as end-wall ventilation, end-wall leakage, and mechanical losses), the design is expected to achieve a maximum efficiency of 75.5% in expander mode at a nominal speed of 1800 rpm. However, a conventional approach has been used to evaluate end wall frictional loss of both sides at zero leakage which is around 16 W. Considering this loss, nominal efficiency drops to around 65.5%. The actual prototype is expected to be further affected by rotor leakage, mechanical losses, electrical losses. Mechanical, structural and dynamic aspects encountered during the design phase are also discussed. These findings are subject to validation through an extensive experimental campaign planned for the near future. Tesla turbine harvester solution for converting the potential energy (pressure) and kinetic energy (flow) of fluids into electricity, on site, seem to be promising and would enable the adoption of intelligent digital solutions in critical infrastructures such as water piping networks.

Acknowledgements

The work presented here has been partially supported by the Italian National project SMART PIPING founded by IREN-AMGA Foundation - Italy.

References

[1] Rice, W., 1965, "An Analytical and Experimental Investigation of Multiple Disk Turbines", Journal of Engineering for Power, Vol. 87(1), pp. 29–36.
[2] Tiwari, R., N., Traverso, A., and Reggio, F., 2023, "Performance Assessment of a Reversible Tesla Machine", E3S Web Conf. Volume 414, 2023, 2nd SUPEHR 23 conferences, Savona, Italy. https://doi.org/10.1051/e3sconf/202341403002.
[3] Tesla, N., 1913, "Turbine", US Patent 1061206.
[4] Tesla, N., 1913, "Fluid propulsion" US Patent 1061142.
[5] Tiwari, R., N., Niccolini Marmont, C., A., Reggio, F., Silvestri, P., Traverso, A., and Ferrari, M., L., "Acoustic Signature Analysis of a Bladeless Blower", *Applied Acoustic*, **Vol-208(6)** (2023), https://doi.org/10.1016/j.apacoust.2023.109382.
[6] Mantelli L, Ferrari M.L., Traverso A., "Dynamics and control of a turbocharged solid oxide fuel cell system", *Applied Thermal Engineering*, 191 (2021) 116862_1-14.
[7] Rice, W., 1963, "An Analytical and Experimental Investigation of Multiple Disk Pumps and Compressors", *J. Eng. for Power,* **85(3)** Pp. 191-198, (1963).
[8] Tiwari, R., N., Reggio, F., Renuke, A., Pascenti, M., Traverso, A., Ferrari, M.L.,"Performance Investigation of a Bladeless Air Compressor" *J. Eng. Gas Turbines Power*, **Vol-144(9) (**2022) https://doi.org/10.1115/1.4054945.
[9] Rice, W., "Tesla Turbomachinery," Handbook of Turbomachinery, Logan, E., and Ray, R., Marcel Dekker, New York, Chap. 14 (2003).
[10] Renuke, A, F. Reggio, P. Silvestri, A. Traverso, Pascenti, M.,"Experimental Investigation on a 3 kW Air Tesla Expander with High-Speed Generator", *ASME Turbo Expo 2020*, virtual, ASME Paper GT2020-14572.
[11] Zhao, D., Ji, C., Teo, C., & Li, S., "Performance of small-scale bladeless electromagnetic energy harvesters driven by water or air", *Energy,* 74, 99-108, (2014).
[12] Silvestri, P., Traverso, A., Reggio, F., Efstathiadis, T. "Theoretical and experimental investigation on rotor dynamic behavior of bladeless turbine for innovative cycles" Proceedings of the ASME Turbo Expo, (2019).
[13] http://www.sit-tesla-technologies.com/, last access 15/05/2024.
[14] Renuke, A., Reggio, F., Traverso, A., Pascenti, M. "Experimental Characterization of Losses in Bladeless Turbine Prototype" *J. Eng. Gas Turbines Power*, 2022, **144(4),** 041009 .
[15] Tiwari, R., Eleftheriou, K., Ferrari, M.L., Efstathiadis, T., Traverso, A., and Kalfas, A., "Numerical Investigation of Bladeless Compressor on Different Disk Spaces and Diffuser Configurations" *J. Eng. Gas Turbines Power*, **Vol-145(01) (**2022**).** doi.org/10.1115/1.4055705.
[16] Tiwari, R., N., Traverso, A., Pascenti, M., and Ferrari, M., L., "Performance Investigation of a Bladeless air Compressor Using Numerical Simulation" ASME Turbo Expo 2023, Paper Number GT2023-102615, (2023).
[17] Galindo, J., Hoyas, S., Fajardo, P., Navarro, R., 2013, "Set-Up Analysis and Optimization of CFD Simulations for Radial Turbines", Engineering Applications of Computational Fluid Mechanics, 7:4, 441-460, DOI: 10.1080/19942060.2013.11015484.
[18] Zhu, Y., and Jiang, P., 2014, "Experimental and Numerical Investigation of the Effect of Shock Wave Characteristics on the Ejector Performance," Int. J. Refrig., 40, pp. 31–42.
[19] Menter, F. R., 1992, "Influence of Freestream Values on k-Omega Turbulence Model Predictions", AIAA J., 30(6), pp. 1657–1659.